A Refined Model of the Thyrotropin-Releasing Hormone (TRH) Receptor Binding Pocket. Novel Mixed Mode Monte Carlo/Stochastic Dynamics Simulations of the Complex between TRH and TRH Receptor†

Liisa J. Laakkonen,‡ Frank Guarnieri,‡ Jeffrey H. Perlman,§ Marvin C. Gershengorn,§ and Roman Osman*,‡

Department of Physiology and Biophysics, Mount Sinai School of Medicine of the City University of New York, New York, New York 10029, and Division of Molecular Medicine, Department of Medicine, Cornell University Medical College and The New York Hospital, New York, New York 10021

Received September 14, 1995; Revised Manuscript Received March 4, 1996⊗

ABSTRACT: Previous mutational and computational studies of the thyrotropin-releasing hormone (TRH) receptor identified several residues in its binding pocket [see accompanying paper, Perlman et al. (1996) *Biochemistry 35*, 7643−7650]. On the basis of the initial model constructed with standard energy minimization techniques, we have conducted 15 mixed mode Monte Carlo/stochastic dynamics (MC−SD) simulations to allow for extended sampling of the conformational states of the ligand and the receptor in the complex. A simulated annealing protocol was adopted in which the complex was cooled from 600 to 310 K in segments of 30 ps of the MC−SD simulations for each change of 100 K. Analysis of the simulation results demonstrated that the mixed mode MC−SD protocol maintained the desired temperature in the constant temperature simulation segments. The elevated temperature and the repeating simulations allowed for adequate sampling of the torsional space of the complex with successful conservation of the general structure and good helicity of the receptor. For the analysis of the interaction between TRH and the binding pocket, TRH was divided into four groups consisting of pyroGlu, His, $ProNH_2$, and the backbone. The pairwise interaction energies of the four separate portions of TRH with the corresponding residues in the receptor provide a physicochemical basis for the understanding of ligand−receptor complexes. The interaction of pyroGlu with Tyr106 shows a bimodal distribution that represents two populations: one with a H-bond and another without it. Asp195 was shown to compete with pyroGlu for the H-bond to Tyr106. Simulations in which Asp195 was interacting with Arg283, thus removing it from the vicinity of Tyr106, resulted in a stable H-bond to pyroGlu. In all simulations His showed a van der Waals attraction to Tyr282 and a weak electrostatic repulsion from Arg306. The $ProNH_2$ had a strong and frequent H-bonding interaction with Arg306. The backbone carbonyls show a frequent H-bonding interaction with the OH group of Tyr282 and strong, often multiple, interactions with Arg306. Three structures, which maintained these interactions simultaneously, were selected as candidates for ligand−receptor complexes. These show persistent interactions of TRH with Ile109 and Ile116 in HX 3 and with Tyr310 and Ser313 in HX 7, which will be tested to refine the structure of the ligand−receptor complex. The superposition of the three structures shows the extent of structural flexibility of the receptor and the ligand in the complex. The backbone of TRH inside the receptor is in an α-helical conformation, suggesting that the receptor, through its interaction with the ligand, provides the energy required for the conformational change in the ligand from an extended to the folded form.

The tripeptide thyrotropin-releasing hormone (TRH,[1] pyroGlu-His-$ProNH_2$) acts through a specific cell surface receptor (TRH-R). TRH-R, which regulates the activity of cells in the anterior pituitary and nervous system, is a member of a large family of transmembrane proteins that couple to G-proteins (GPCR). Although much progress has been made in constructing molecular models of GPCRs, understanding the molecular mechanism of receptor action remains unclear. Two important elements in such a mechanism are the understanding of the specificity of ligand recognition by the receptor and the activation of the receptor that results from the formation of a ligand−receptor complex. The importance of the first element is in the discrimination of ligands specific for the particular receptor from all other molecules. The significance of the second element can be illustrated by the consequence of the interaction with an agonist which leads to receptor activation as opposed to the interaction with an antagonist which prevents the action of agonists. Thus, the identification of the residues in the receptor which are responsible for such remarkable selectivity is essential for formulating a detailed molecular mechanism of receptor action.

† This work was supported by National Institutes of Health Grant DK 43036 (to M.C.G. and R.O.), Grant T32 DA 07135 (to F.G.), and Physician Scientist Award DK 02101 (to J.H.P.).

* To whom correspondence should be addressed: Department of Physiology and Biophysics, Box 1218, Mount Sinai School of Medicine, One Gustave L. Levy Place, New York, NY 10029.

‡ Mount Sinai School of Medicine of the City University of New York.

§ Cornell University Medical College and The New York Hospital.

⊗ Abstract published in *Advance ACS Abstracts,* June 1, 1996.

[1] Abbreviations: TRH, thyrotropin-releasing hormone; TRH-R, thyrotropin-releasing hormone receptor; MC−SD, mixed mode Monte Carlo/stochastic dynamics; pyroGlu, pyroglutamyl; GPCR, guanine nucleotide-binding protein coupled receptor; HX, transmembrane helix.

S0006-2960(95)02203-3 CCC: $12.00

Two main problems present themselves in identifying the binding pocket in the receptor. Perhaps the most important is the lack of a confident structure for the TRH-R which can serve as a guide for experimental and computational studies to identify the residues involved in binding the ligand. The other problem is the collection of the conformational states of the ligand and the receptor. Both are flexible molecules with many possible accessible states, but there is no clear way of deciding which are relevant to binding. For example, TRH is a flexible molecule with six rotatable bonds, and although its structure is known in a crystal and partly in solution, the conformation it would take when bound to the receptor is not clear. A similar argument, albeit without much specific evidence, can be made about the receptor protein.

To develop a combined theoretical/experimental approach to the understanding of ligand−receptor interaction, we have conducted several mutational and computational studies, which resulted in the identification of several residues in the binding pocket of the receptor. We have demonstrated that the high-affinity binding between the ligand and the TRH-R is retained when the negatively charged Asp residues are mutated to Ala (Perlman et al., 1992). We have previously demonstrated that Tyr106 makes a direct hydrogen-bonding interaction with the C═O group of pyroGlu (Perlman et al., 1994b). On the basis of this finding, preliminary modeling of the receptor identified Asn110 in HX 3 as another potential residue that could interact with the N−H group of the pyroGlu residue of the ligand. This suggestion was confirmed by a complementary mutation of the receptor and the ligand and served as the basis for the construction of an initial binding pocket in the receptor (Perlman et al., 1994a). An important observation from the early model was that Tyr282 in HX 6 could serve as a lid over the ligand in the complex. The importance of the positively charged arginines in HX 6 and HX 7 was also investigated by mutational studies (Perlman et al., 1995). However, while mutations of Arg283 in HX 6 and Arg306 in HX 7 resulted in decreased binding affinities, we did not demonstrate that they interact with a specific part of the ligand. In contrast to Arg306 whose mutation only affected binding affinity, Arg283 in HX 6 was also found to be involved in receptor activation. Mutations of Arg283 to Glu, Ser, or Leu produced nonactivatable receptors, whereas mutations to Lys or His retained a significant amount of receptor activity. The models of the binding pocket that were produced in the course of early studies were not sufficiently robust primarily because the roles of Tyr282 and Arg306 in ligand binding had not been identified specifically. In our recent mutational experiments, we determined that Tyr282 and Arg306 interact with the His and ProNH_2 of the ligand, respectively (Perlman et al., 1996). These data served as the initial conditions for the design of a detailed computational study of the binding pocket of the receptor.

To address the problem of the interaction of a flexible ligand, TRH, with a binding pocket in the TRH receptor that might possess its own conformational flexibility, we decided to utilize a novel technique that combines stochastic dynamics with intervening Monte Carlo steps, a mixed mode MC−SD (Guarnieri & Still, 1994; Guarnieri, 1995). The critical aspect of the simulation method used in the study of the binding pocket is its ability to explore simultaneously many thermally accessible conformational states of the receptor and the ligand. Attempts to enhance sampling have to take into account that intramolecular motions in large systems take place on a multiple time scale because bond stretching and bending occur on a femtosecond to picosecond time scale, whereas torsional rotations around flexible bonds occur on a nanosecond time scale. Thus, an efficient algorithm should be able to sample local wells as well as cross large energy barriers and yield a correct population distribution. Recently, such an approach was applied to a conformational analysis of tetrapeptides containing a proline or other *N*-methylamino acids as determinants of a reverse turn (Chalmers & Marshall, 1995). The authors demonstrate that the mixed Monte Carlo/stochastic dynamics, with an implicit representation of water, yields results that are consistent with experimental studies of tetrapeptides in solution.

The methods and approaches to ligand docking have been recently reviewed (Lybrand, 1995). Several attempts to construct a ligand−receptor complex have been undertaken; however, only a few incorporated ligand and receptor flexibility in their simulations. In an approach based on the availability of the crystal structure of the protein, Rosenfeld et al. (1993) utilized multiple copies of a flexible peptide to derive a structure of the form bound to a class I major histocompatibility complex receptor. In this study, although the ligand was allowed to be flexible, the receptor was kept rigid. In a different approach Zacharias et al. (1994) used a Monte Carlo method to generate a large number of conformations of the flexible arm of the λ repressor in a complex with the DNA operator and then evaluated the electrostatic energy of the accepted conformations with a finite-difference Poisson−Boltzmann approach. The DNA and the rest of the protein remained rigid as in the crystallographic structure. An attempt to include the flexibility of a part of the receptor site was accomplished via a systematic search of side chain conformations of both the ligand and part of the receptor (Leach, 1994) without minimization of the resulting structure. A somewhat different variant of this method first searches the flexible conformations of the ligand and subsequently minimizes the complex to allow for receptor flexibility (Yamada & Itai, 1993a,b).

We present here an extensive computational study of the binding pocket of the TRH-R using the mixed mode MC−SD. Since this is a first application of the technique to a large system, we present an analysis of the technical aspect of the simulations to demonstrate its limits of applicability. We further analyze the results of the simulations in terms of interaction energies which lead to a translation of specific receptor−ligand contacts to a more general molecular description based on the chemical nature of the interacting groups. Finally, we use the structures that result from the simulations to identify additional potential groups that contribute to binding the ligand.

METHODS

Construction of the Starting Structure of the Complex. The construction of the initial complex between TRH and the TRH-R is described in the accompanying paper (Perlman et al., 1996). The initial complex shows that the TRH is positioned in the transmembrane domain and the pyroGlu of TRH forms H-bonds with Tyr106 and Asn110 of the TRH-R. Tyr282 forms a stacking interaction with His of TRH, and Arg306 forms H-bonds with the ProNH_2 and the

backbone carbonyl of pyroGlu. The stability of the initial structure suggested that it could serve as a good starting point to conduct the mixed mode simulations to allow for the exploration of ligand and receptor flexibility.

Mixed Mode Simulations. The structure built with manual docking and minimization was used as a starting structure for an extensive simulation of the binding pocket. The critical aspect of the simulation method used in this study is its ability to explore many thermally accessible conformational states of the receptor and the ligand. Among the methods that explore configuration space are Metropolis Monte Carlo sampling techniques (Metropolis et al., 1953) and molecular dynamics simulations (McCammon & Harvey, 1987). A recently developed efficient algorithm combines stochastic dynamics (SD) in Cartesian space with Metropolis Monte Carlo sampling in torsion space (MC−SD) (Guarnieri & Still, 1994). In this method, after every dynamics step a random trial torsional deformation is performed and accepted or rejected according to the Metropolis criteria. Regardless of the outcome of the Metropolis test, the next step is computed from the current configuration using the velocities from the previous dynamical step. This method is radically different from other schemes that introduce a dynamical step to produce a new trial configuration for the Monte Carlo sampling. The mixed mode MC−SD actually merges the algorithms of dynamics and Monte Carlo, essentially eliminating the distinction between deterministic and stochastic simulations.

Because of the novelty of this approach a succinct description of the simulation algorithm is provided here. A complete description was recently published (Guarnieri, 1995).

The stochastic equation of motion is

$$m\frac{\mathrm{d}\nu}{\mathrm{d}t} = f[x(t)] + R(t) - m\gamma\nu$$

where m is the mass of the particle, υ the velocity, x the position, f the deterministic force, γ the friction coefficient, and R the random force due to solvent.

The time correlation of the random variables assuming δ-function memory is

$$\langle R(t)R(t')\rangle = 2m\gamma kT\delta(t - t')$$

where t is time, k is Boltzmann's constant, T is the temperature, and the brackets indicate ensemble averaging.

The important aspect of this method is the computation of new velocities according to the velocity Verlet algorithm (Swope et al., 1982), which is a forward-looking algorithm and thus is most compatible with an intervening MC step in a SD simulation. It successfully avoids the discontinuities in positions and forces that will be produced by intervening MC steps into other dynamics integration schemes. The new positions and velocities are calculated as

$$x(t + \Delta t) = x(t) + \frac{\nu(t)}{\gamma}(1 - \mathrm{e}^{-\gamma\Delta t}) + \frac{f[x(t)]}{m\gamma^2}(1 - \mathrm{e}^{-\gamma\Delta t}) + R1(t, t + \Delta t)$$

$$\nu(t + \Delta t) = \nu(t)\mathrm{e}^{\gamma\Delta t} + \frac{f[x(t)] + f[x(t + \Delta t)]}{2m\gamma}(1 - \mathrm{e}^{-\gamma\Delta t}) + \frac{R1(t, t + \Delta t) + R1(t + \Delta t, t + 2\Delta t)}{2\Delta t} + \frac{R2(t - \Delta t, t) + R2(t, t - \Delta t)}{2\Delta t}\mathrm{e}^{-\gamma\Delta t}$$

where

$$R1(t, t + \Delta t) = \frac{1}{m\gamma}\int_t^{t+\Delta t} R(t')(1 - \mathrm{e}^{-\gamma(t-t')})\,\mathrm{d}t'$$

and

$$R2(t, t + \Delta t) = \frac{1}{m\gamma}\int_t^{t+\Delta t} R(t')(\mathrm{e}^{-\gamma(t-t')} - 1)\,\mathrm{d}t'$$

are the stochastic forces.

As can be seen from the equations, the position integration to $x(t + \Delta t)$ only requires knowledge of $x(t)$. The velocity integration requires knowledge of forces at time t and $t + \Delta t$, but not at $t - \Delta t$. Thus, accepting a MC step and loading the positions into $x(t)$ will not cause a discontinuity because calculation of the new positions, velocities, and forces does not require knowledge of the positions at $x(t - \Delta t)$.

The method is driven by the following algorithm:

For a given initial structure, initial velocities are assigned, initial deterministic forces are computed, and initial forces due to the random variables are assigned. New positions and forces are computed according to SD velocity Verlet algorithms. A MC step on the torsional variables is attempted, and if successful, the new coordinates are loaded into $x(t)$; if the MC step is not accepted, a SD step is taken with previous coordinates. This method has been shown to produce converged canonical ensembles in model systems (Guarnieri & Still, 1994) with convergence rates that are about 2−3 orders of magnitude faster than other simulations. The method is incorporated in MacroModel (Mohamadi et al., 1990) and uses the modified AMBER* force field (Weiner & Kollman, 1981; Weiner et al., 1984).

Simulation Procedure. The system of the receptor model with the ligand consists of 189 residues and 1678 atoms in an extended atom representation. Because the entire system contains too many torsional angles to be varied in the Monte Carlo part of the mixed mode MC−SD, a certain portion of the system was delimited to be an MC-active zone. Thus, in the mixed mode simulation the stochastic dynamics steps are performed on the entire system whereas the Monte Carlo steps only on the MC-active zone. The set of torsional angles to be varied by the Monte Carlo steps was chosen to include all nonpeptide torsional angles of the ligand and all side chain torsional angles of the residues that had at least one atom within a sphere of 6 Å from any atom of the ligand. The MC-active zone of the receptor, shown in Figure 1, consisted of 46 residues with 97 free torsional angles. Five torsional angles were selected randomly at each Monte Carlo step to be changed by a value between −30° and +30°. The acceptance rate was 17% at 700 K and decreased to 10% at 310 K. Initial trial runs with a smaller active zone resulted in an acceptance rate of approximately 4%. The small active zone, in addition to not being spherical, has many more MC-

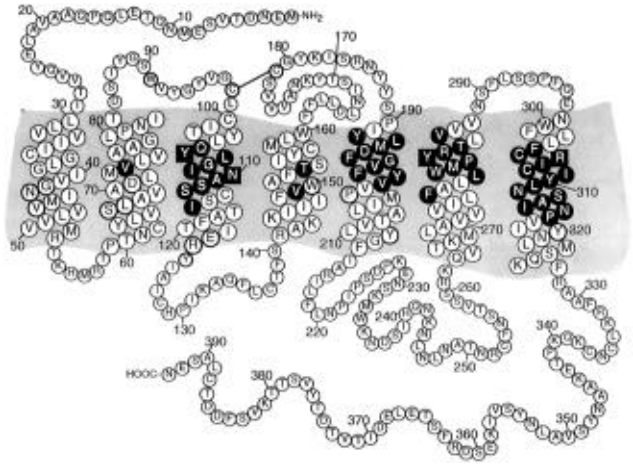

FIGURE 1: Schematic description of the helical domains of TRH-R. The shaded area represents the lipid and the Monte Carlo active zone is highlighted in black. The residues used for guiding the construction of the ligand−receptor complex are shown in squares.

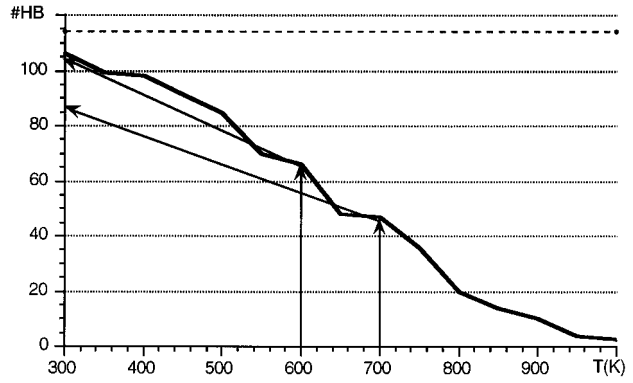

FIGURE 2: Number of α-helical H-bonds as a function of temperature. The broken line represents the total number of α-helical H-bonds in the minimized structure. Two starting temperatures for cooling are depicted by vertical arrows, and their result is shown by the arrows on the ordinate.

inactive residues surrounding the MC-active zone. Most probably, the MC steps are rejected more often because a simultaneous change of several dihedral angles is not possible with the smaller active zone. The cutoff distance for nonbonded interactions was increased to 30 Å, which corresponds to the largest separation between any two atoms in the ligand−receptor complex in an extended conformation. Without this change, a constant temperature cannot be maintained in the simulations because of overheating. The time step in the simulations was 1.5 fs, and MC and SD steps were attempted in 1:1 ratio. The surroundings of the complex were described by a distant-dependent dielectric, which is default for AMBER* parameters in MacroModel.

To enhance sampling of conformational space and to reduce dependence on the starting structure, a simulated annealing protocol was developed (Kirkpatrick et al., 1983). To decide about the starting temperature of the annealing, the receptor−ligand complex was heated to 1000 K by steps of 50 K, with 2 ps of stochastic dynamics at each temperature. The number of α-helical backbone H-bonds was monitored as a function of temperature. Figure 2 shows the number of α-helical H-bonds (from residue i to $i + 4$) as a function of temperature. The minimized structure has 113 α-helical H-bonds (shown as a broken line), which diminished progressively as the temperature increased. At 1000 K, even though practically all α-helical H-bonds were lost, the bundle of peptide chains stayed together. At 700 K the system retained 47 α-helical H-bonds, which is a little less than half of the H-bonds at 300 K. However, annealing from 700 to 310 K regenerated only 87 helical H-bonds (see Figure 2). When cooling started from 600 K, with 66 initial H-bonds, nearly all H-bonds were re-formed, resulting in good helical peptide strands. Consequently, all simulated annealings were started at 600 K and cooled to 310 K in four steps of 100 K each. At each temperature the system was simulated for 30 ps with a coupling constant of 0.4 ps. The overall time of each simulation was 120 ps. Fifteen separate simulations were performed, each with a different seed for the random number generator. This is probably not sufficient to reach numerically converged results in such a large complex, but the simulation results show recurring structural features indicating an adequate sampling of the torsional space in the MC-active zone.

To reduce excessive fluctuations of the ligand, a weak flat-bottomed constraint [see Perlman et al. (1996)] was imposed between the O−H (Tyr106) and the ring C═O (pyroGlu) of the ligand. The constraining force constant was 50 kJ/Å^2, and the optimal distance r_0 was 2.5 Å with a tolerance of ±0.5 Å. This is not restraining the structure excessively, judged by the fact that in several simulations O−H (Tyr106) turned away from a H-bonding configuration while attracted to other groups in the vicinity (see below). A specific distant constraint cannot be imposed on the Tyr282−His interaction because it is governed mostly by van der Waals forces which are not localized to specific atoms. Likewise, the interaction between the multipronged guanidinium group of Arg306 with the C═O of ProNH$_2$ could not be limited to one specific set of atoms and thus was not constrained. Distance monitors were set between Tyr106, Tyr282, and Arg306 in the receptor and pyroGlu, His, and ProNH$_2$ in TRH, respectively. Angle monitors were set for all the torsions of the ligand.

RESULTS AND DISCUSSION

The analysis of the results from the simulation concentrates on three different aspects.

(1) The novelty of the application of the mixed mode MC−SD methodology to such a large system as the ligand−receptor complex required an evaluation of the performance of the mixed mode method in the present circumstances. The helical bundle used in this study is made of seven independent helices, and it lacks certain constraints that are present in the complete system. The connecting loops, both extra- and intracellular, are not present in this structure, and the additional kinetic energy at high temperature might contribute to the dissociation of the bundle. Also, the environment of the bundle, i.e., the phospholipid membrane, has been simulated in an unsophisticated way as a continuum dielectric that scales the nonbonded interactions by the distance between the interacting atoms. Thus, the evaluation of the overall structure with the particular emphasis on the intactness of the helices and the bundle is required.

(2) The main question addressed by this study was the structure of the binding pocket and the nature of ligand−residue interaction. We present below an energetic analysis to establish a mechanistic representation of the specificity of ligand receptor interaction.

(3) The dynamical/stochastic nature of the simulations allows us also to present the extent of the fluctuations in the structure and the possible mobility of the ligand and the receptor.

The Simulation Protocol. Because of the intervening Monte Carlo steps in the mixed mode MC−SD simulation protocol, the constancy of temperature in the simulation segments that have been designed in the protocol is a good indicator of a properly executed simulation. In all 15 simulations, the temperature changed rapidly from one target temperature to another and remained quite stable throughout the constant temperature segments. The total energy changed in a parallel fashion with the temperature showing a slight delay behind the changes in the temperature. Also, in the course of the constant temperature segments the energy kept drifting to lower values as is expected from a stochastic dynamics with intervening Metropolis MC steps. The behavior of the temperature and the total energy in a representative run is shown in Figure 3.

Another reason to choose the mixed mode MC−SD method and to conduct simulations at elevated temperatures was to ensure good sampling of the conformational space in the complex. The success of such a procedure was evaluated from temperature dependence of fluctuations in ligand dihedral angles and from the number of major changes in their values at different temperatures. The total number of changes $\geq 60°$ in the dihedral angles in all the runs is 53, with 12 occurring at 300 K and the rest at the higher temperatures of 500 and 600 K. Figure 4 shows a representative plot of the evolution of three dihedral angles in the ligand, ψ_1, χ_1, and χ_2, throughout the entire course of a single simulation [see Laakkonen et al. (1996) for the structure of TRH with angles shown]. For the purpose of comparison, the fluctuations in ϕ_1, an angle that is constrained inside the pyroGlu ring, is shown to demonstrate the range of fluctuations in an angle that cannot change freely. Clearly, the mixed mode simulation protocol enhances conformational mobility as illustrated by the changes in the torsional angles. A similar conclusion is reached from the study of fluctuations in structural parameters. The fluctuations of the angles in the ligand and of the monitored distances between the ligand and the residues in the receptor were calculated in each 1 ps segment throughout the simulation, and their behavior was examined. At higher temperatures the fluctuations were larger that at the lower temperatures. For example, the average value of ϕ_2 in one of the simulations was $-73 \pm 18°$ at 600 K, and it changed to $-59 \pm 10°$ at 310 K. In another simulation, the value of ψ_3 was $-78 \pm 18°$ at 600 K, and it changed to $-106 \pm 14°$ at 310 K, whereas that of χ_1 was $-87 \pm 25°$ at 600 K, and it changed to $-60 \pm 7°$ at 310 K. Similar behavior is observed for the monitored distances. Clearly, the fluctuations indicate that sampling is performed and the effect of temperature, although not large, is consistent and independent of the direction of the changes in the average values.

The examination of the populations of the dihedral angles of TRH and their dependence on number of simulations and temperature show the advantage of conducting multiple runs and using elevated temperatures. There are six free dihedral angles in TRH. Their distribution at 310 K, derived from 30 000 configurations combined from all simulations, is shown in Figure 5a. For comparison, Figure 5b shows a distribution at all temperatures from a single run derived from

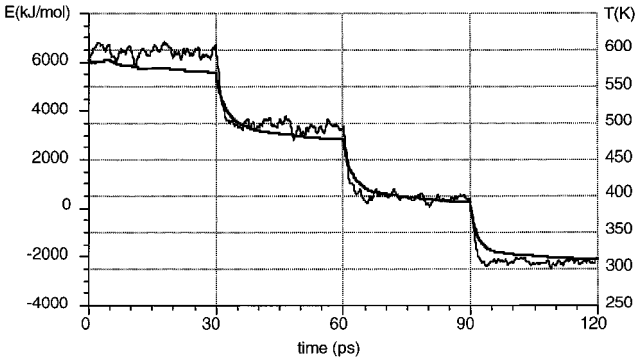

FIGURE 3: Example of the changes in energy (kJ/mol, thick line) and temperature (K, thin line) as a function of time during a simulated annealing run.

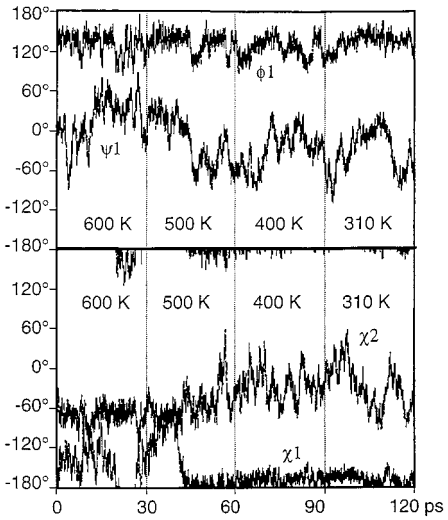

FIGURE 4: Example of time course of changes in selected torsional angles of TRH inside the receptor during a simulated annealing run. Note that χ_1 starts at $-60°$ and changes to $-180°$ around 40 ps. χ_2 starts at $-150°$ and changes to $-50°$ in a gradual fashion between 30 and 50 ps.

8000 configurations and Figure 5c a distribution of the angles at 310 K from a single run derived from 2000 configurations. The distributions in Figure 5a show that the free angle of pyroGlu, ψ_1, has a wide distribution that covers nearly the complete dihedral space, with preferred populations around 30° and $\pm 150°$. The backbone dihedrals of His, ϕ_2 and ψ_2, are localized around $-60°$, forming an α-helical turn in the peptide. The distribution of ψ_2 is very narrow whereas that of ϕ_2 could probably be decomposed into two unevenly populated distributions, the major at $-60°$ and the minor at $-120°$. The His side chain angle χ_1 shows a trimodal distribution with a very small population at $+60°$ and χ_2 a bimodal behavior, with maxima at $+60°$ and $-120°$. Such a distribution is consistent with the nature of these bonds. The free angle of Pro, ψ_3, shows a broad and asymmetric distribution around 150°, suggesting a minor population at $-120°$. It is interesting to compare the distribution from a single run either at all the temperatures (see Figure 5b) or at 310 K (see Figure 5c) to that obtained from the entire set of runs at 310 K (see Figure 5a). Clearly, one run at 310 K is not sufficient to sample a representative distribution of dihedral angles within the 30 ps simulation time. The distributions are localized around single values, which can be found in the total distribution (see Figure 5a), but they do not provide a way of evaluating their relative importance

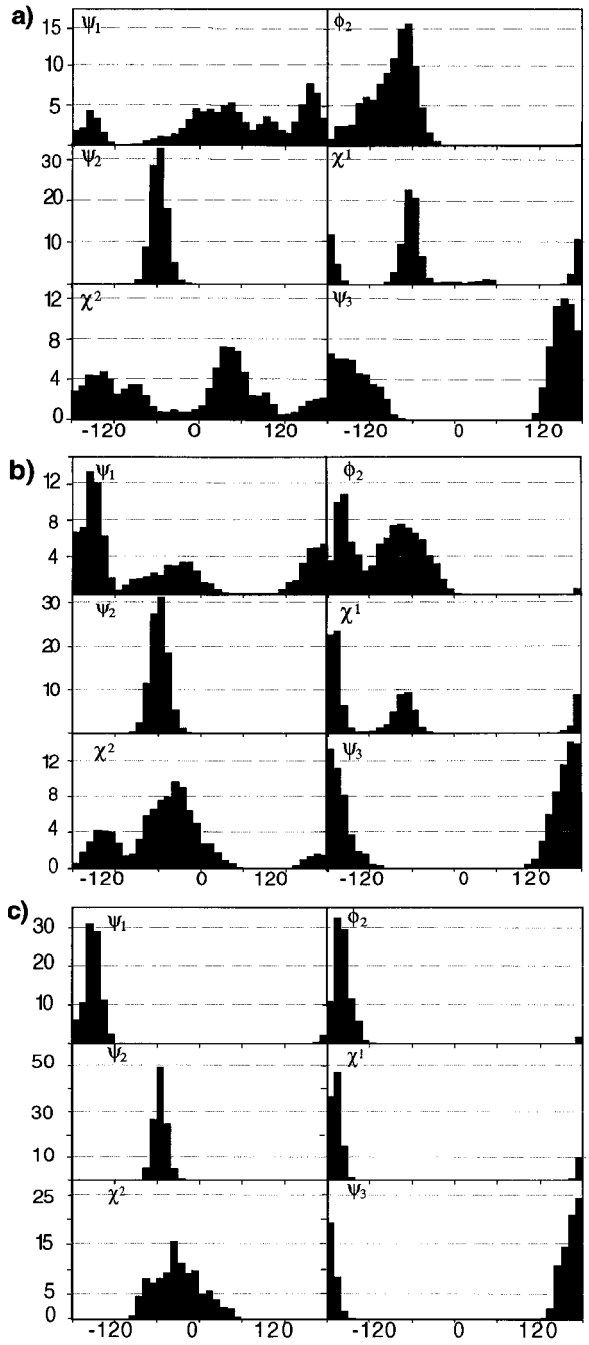

FIGURE 5: Distribution of the six torsional angles of TRH inside the receptor in the course of simulated annealing. The *x*-axis shows the values of the angles in the range −180° to +180° and the *y*-axis the fractional population in percentages. The angles have been monitored every 1.5 fs. Panels: (a) distribution from 30 000 structures from 15 simulations at 310 K; (b) distribution from 8000 structures from 1 simulation at all the temperatures; (c) distribution from 2000 structures from 1 simulation at 310 K.

with respect to other regions of torsional space. On the other hand, the distribution of dihedral angles sampled at all temperatures in a single run is very similar to that at 310 K. Thus, we conclude that multiple simulated annealing runs sample the conformational space in an exhaustive way and provide a representative distribution of structures.

The General Structure of the Receptor. The integrity of the complex in the course of the simulations was evaluated by measuring the volumes of the final structures, which were all within 1% of the mean. The final structures had decreased in volume on the average by 7% compared to the starting structure. This small change is most probably caused by the lack of a realistic environment in the simulations. For structural evaluation of the helices, the number of helical H-bonds in the final structures was calculated at 310 K. On the average, 87% of the helical H-bonds of the minimized starting structure were maintained in all simulations. Despite the conservation of volume and good helicity, overall changes were observed in the structure. The helical ends, both at the top and the bottom, frayed or unwound nonsystematically. Since the simulations addressed the nature of the binding pocket, which is entirely enclosed within the transmembrane domain, such changes were not considered alarming. The helical ends were observed to tilt toward the bundle, as if to minimize the exposed area at the ends of the helices. This is also most probably caused by the nonrealistic representation of the environment. Helix 4, which is lying on the outside of the bundle and has strong positive charges at the intracellular end, showed the largest distortions. Yet, since no residue from this helix is part of the binding pocket, such changes in the helix may have only a small effect. Simulations with lipids that contain polar head groups would likely stabilize helix 4 and the entire bundle.

The binding pocket does not deform greatly. The ligand moves relative to the helices, but it stays inside the binding pocket in all runs. This is expected because the packing around TRH is relatively tight. A comparison of the starting structure for the simulations to selected final structures of the complex (see below) shows that the root mean square deviation of the C_α ranges from 3.6 to 4.3 Å. TRH moves in a counterclockwise direction when the bundle is viewed from the extracellular side. The extent of the movement determined from the center of mass of TRH ranges from 2 to 4 Å. Individual residues of TRH move from their original position and form new interactions. The specific interactions of pyroGlu, His, and $ProNH_2$ are described in detail below; here we concentrate only on the interactions that changed from the initial structure. The major and consistent change is the repositioning of the imidazole ring of the His residue of TRH. Originally it was positioned between HX 5 and HX 6, but in the course of the simulations it rotated to a position between HX 6 and HX 7 close to Leu274. This was accomplished by a large change in ψ_1 (∼100°) and a smaller change in ϕ_2 (∼40°). Since Tyr282 maintained its interaction with His throughout the simulations, this residue followed the imidazole ring, inducing a slight rotation of HX 6. In some simulations the original H-bond of the pyroGlu backbone carbonyl group to Arg306 is broken and replaced by various other H-bond donors, e.g., the OH of Tyr282 or the backbone NH of Phe196. The carbonyl group of the $ProNH_2$ maintained its interaction with Arg306, but the amino group moved to form H-bonds with residues in the space between HX 2 and HX 7, e.g., Asp71, Ser112, Tyr310, and Ser313.

Thus, the general shape of the receptor bundle and the behavior of the extremities of the helices does not present a problem in studying the binding pocket. The erratic behavior of the helix ends emphasizes the need to construct a complete model of the receptor, which will include the extra- and intracellular loops. Also, a more realistic description of the environment, while not practical at this time, would probably prevent some of the distortions observed in the helices. The general changes in the position of the ligand in the binding pocket suggest that the mixed mode simulation procedure

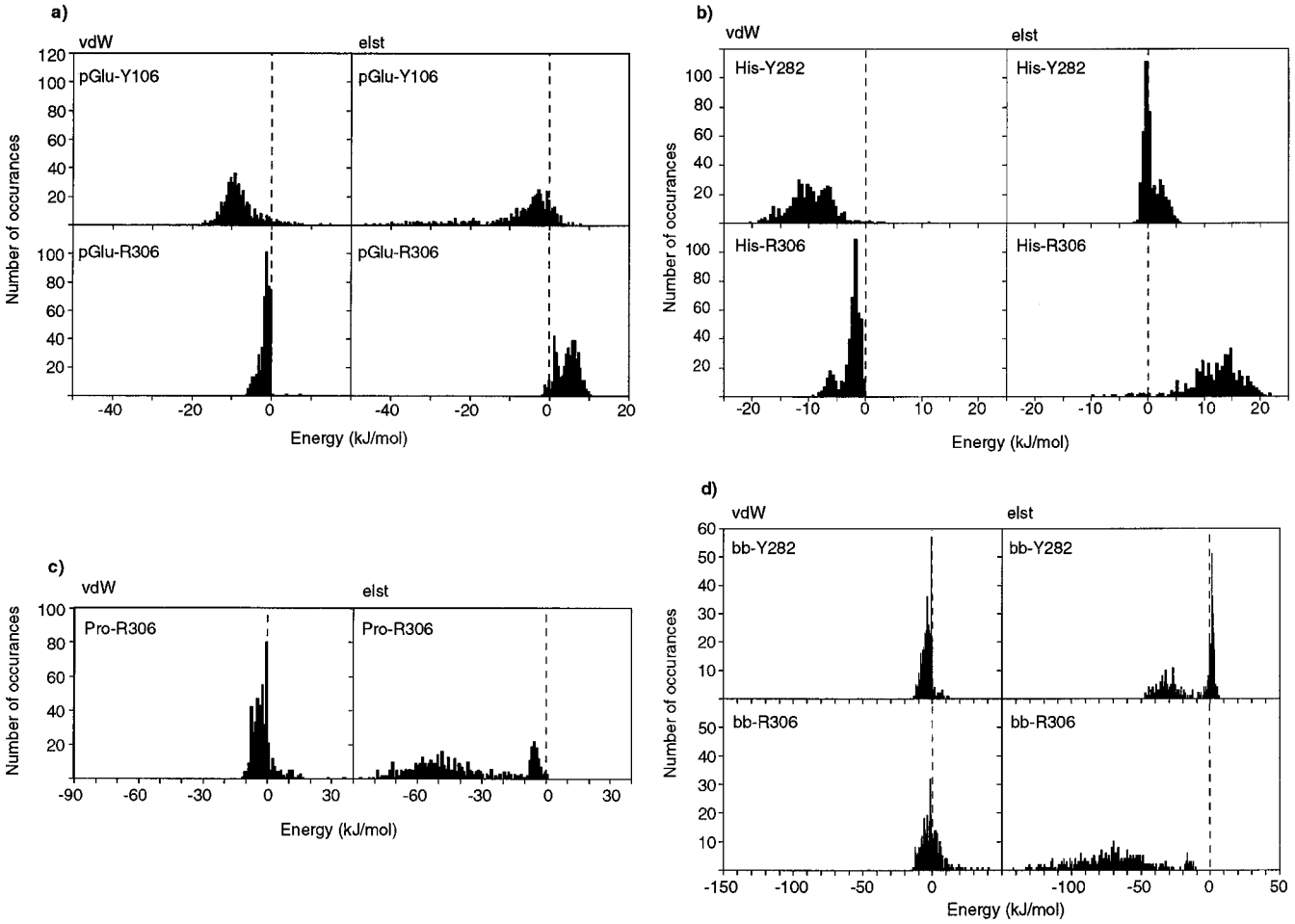

FIGURE 6: Distribution of pairwise nonbonded interaction energies divided into van der Waals (vdW) and electrostatic (elst) contributions. Panels: (a) interactions of pyroGlu of the ligand with Tyr106 (Y106, top panels) and Arg306 (R306, bottom panels); (b) interactions of His of the ligand with Tyr282 (Y282, top panel) and Arg306 (R306, bottom panel); (c) interactions of $ProNH_2$ of the ligand with Arg306 (R306); (d) interactions of backbone (bb) of the ligand with Tyr282 (Y282, top panels) and Arg306 (R306, bottom panels). See text for definition of the various parts of the ligand.

allowed for good sampling of the environment of the binding pocket.

Binding Pocket. To characterize the binding of TRH in the binding pocket, we analyzed the interaction energies between the various portions of the ligand and the respective residues in the receptor. The ligand was divided into four parts: three consisted of each side chain that included the C_α atom and the fourth group consisted of the backbone atoms, i.e., two carbonyl groups and one N−H. The carboxamide terminus was considered as part of proline. This division attempts to partition the TRH molecule in an analogous way to the experimental testing of ligand−receptor interactions. In experimental conditions, each side chain can be modified separately as demonstrated in the replacement of pyroGlu by Pro to eliminate the C═O group (Perlman et al., 1994b) or the replacement of His by Phe in TRH or by eliminating the terminal carboxamide by converting the $ProNH_2$ by a pyrrolidine ring [see Perlman et al. (1996)]. Since changes in the backbone are harder to construct, the present study may serve to predict the importance of the backbone to ligand−receptor interaction. The nonbonded interactions are divided into van der Waals and electrostatic contributions. We have analyzed the interactions from all the simulation segments at 310 K sampled every 1 ps. This yields 450 values for each distribution. The distributions of the pairwise interaction energies are shown in Figure 6a−d. The interaction with pyroGlu are shown in Figure 6a, with His in Figure 6b, with $ProNH_2$ in Figure 6c, and with the backbone in Figure 6d. The individual average energy values for each of the 15 simulations are shown in Table 1. The interaction energies between Tyr106 and His, Pro, or backbone are not included because they are smaller than 0.5 kJ/mol.

Pyroglutamate of TRH. As can be seen from Figure 6a, pyroGlu shows only significant interactions with Tyr106 and Arg306. The distribution of the electrostatic interaction energies between pyroGlu and Tyr106 shows a bimodal distribution with a large population centered around −3.4 kJ/mol and a smaller distributed population ranging from −13 to −46 kJ/mol with a mean of −21 ± 10 kJ/mol. The population with the strong electrostatic interaction represents all the structures with a Tyr106−pyroGlu H-bond, which was inferred from experimental data and used to guide the placement of the ligand in the binding pocket. However, the structures with an intact H-bond represent only 27% of the entire distribution; i.e., they are observed in only 4 out of 15 simulations (see Table 1A, simulations 3, 9, 11, and 12). In the rest of the cases Asp195 from the upper part of helix 5 forms a strong ionic H-bond with Tyr106 and supplants the original Tyr106−pyroGlu interaction. In the runs in which the Tyr106−pyroGlu H-bond was intact, Asp195 interacts with other parts of the receptor. The

Table 1: Pairwise Interaction Energies

(A) Pairwise Interaction Energies (kJ/mol) between pGlu of TRH and the Residues in the Receptor

	Tyr106		Arg306			Tyr106		Arg306	
simulation no.	vdW	elst	vdW	elst	simulation no.	vdW	elst	vdW	elst
1	−7.8	−4.3	−0.8	1.7	10	−9.5	−3.9	−1.5	7.0
2	−4.4	−1.3	−1.6	5.1	11	−9.8	−11.2	−3.4	8.0
3	−6.9	−23.0	−0.5	1.7	12	−9.8	−15.5	−1.6	4.3
4	−4.6	−1.9	−0.3	−0.6	13	−10.0	1.3	−2.9	5.7
5	−9.7	−7.6	−4.0	5.7	14	−11.6	−4.7	−3.1	7.4
6	−12.9	−1.9	−1.6	7.0	15	−6.8	−4.9	−1.9	2.7
7	−7.8	−3.0	−1.0	4.2					
8	−7.9	−5.7	−1.0	5.3	av energy	−8.1	−8.1	−1.7	4.4
9	−1.3	−33.9	−0.2	1.2	std dev	3.0	9.4	1.2	2.6

(B) Pairwise Interaction Energies (kJ/mol) between His in TRH and the Residues in the Receptor

	Tyr282		Arg306			Tyr282		Arg306	
simulation no.	vdW	elst	vdW	elst	simulation no.	vdW	elst	vdW	elst
1	−9.2	0.0	−1.2	11.2	10	−9.1	−0.4	−2.9	13.0
2	−9.3	−0.1	−2.0	13.7	11	−7.2	3.8	−0.6	9.4
3	−11.2	1.5	−1.7	9.4	12	−4.5	1.5	−1.7	12.3
4	−12.0	2.6	−0.7	−5.8	13	−12.0	2.8	−5.4	9.9
5	−6.2	−0.2	−2.9	18.1	14	−10.1	−0.9	−1.9	16.8
6	−11.3	−0.4	−2.2	14.3	15	−9.4	−0.4	−5.7	16.8
7	−12.2	1.7	−1.7	14.3					
8	−13.9	−0.8	−2.2	14.6	av energy	−9.6	0.7	−2.6	12.0
9	−6.4	0.3	−6.7	0.4	std dev	2.6	0.4	1.9	4.6

(C) Pairwise Interaction Energies (kJ/mol) between $ProNH_2$ in TRH and the Residues in the Receptor

	Arg306			Arg306	
simulation no.	vdW	elst	simulation no.	vdW	elst
1	−1.9	−65.5	10	−4.1	−43.1
2	−4.3	−49.3	11	−0.8	−5.5
3	−1.6	−49.2	12	−5.4	−30.3
4	−0.6	−3.0	13	−2.2	−55.9
5	3.4	−64.7	14	−3.3	−32.9
6	−0.6	−50.8	15	−1.0	−52.8
7	0.0	−49.8			
8	−2.1	−6.0	av energy	−2.0	−39.1
9	−5.6	−27.2	std dev	2.3	20.8

(D) Pairwise Interaction Energies (kJ/mol) between the Backbone of TRH and the Residues in the Receptor

	Tyr282		Arg306			Tyr282		Arg306	
simulation no.	vdW	elst	vdW	elst	simulation no.	vdW	elst	vdW	elst
1	−4.5	−3.4	−1.0	−63.3	10	−2.8	1.5	−1.6	−94.3
2	−1.5	0.7	4.6	−95.1	11	−3.8	−29.9	−1.3	−65.6
3	−1.1	−30.8	−2.2	−44.0	12	−7.2	−24.7	4.7	−96.5
4	−3.0	−29.2	−1.3	−15.1	13	−3.4	−33.2	−6.0	−53.6
5	−2.6	2.4	−5.3	−65.8	14	−3.2	1.6	−1.6	−93.6
6	−8.5	−1.1	−5.6	−59.9	15	−0.8	−0.4	−8.0	−75.8
7	−4.8	−33.3	1.0	−66.1					
8	−6.2	2.2	5.0	−111.9	av energy	−3.6	−11.8	−1.2	−71.4
9	−0.7	0.5	0.4	−70.2	std dev	2.3	15.7	4.0	24.5

interaction partners of Asp195 vary and include the N−H of the indole ring of Trp150 in helix 4, the O_γ−H of Thr153 in helix 4, the backbone N−H groups of Gly197, Val198, and Phe199 in helix 5, and both backbone and side chain N−H of pyroGlu of the ligand. It appears that in the present model of the receptor the position of Asp195 presents an attractive competitive site for Tyr106, thus reducing the probability of maintaining the Tyr106−pyroGlu H-bond. To test this suggestion, we placed the side chain of Asp195 close to Arg283 in helix 6 and minimized the structure. The electrostatic interaction between the oppositely charged residues ensures a strong bond which will keep Asp195 away from Tyr106. Four mixed mode MC−SD simulations were performed on this complex and analyzed for the existence of the Tyr106−pyroGlu H-bond. In all four simulations a strong Tyr106−pyroGlu H-bond persisted. The distributions of the Tyr106−pyroGlu pairwise interaction energies in these runs are shown in Figure 7. The nearly symmetrical distribution is centered at -25.4 ± 6.3 kJ/mol without any presence of the low interaction energies that appeared in the previous runs. All other pairwise interaction energy distributions to the other residues of TRH are similar to those shown in Figure 6b−d. Another noticeable change that accompanies these simulations is the restriction of two torsional angles to a limited region. The sampling of ψ_1 is limited to a range between 0° and 60° with a higher frequency toward the upper end of the values. The other angle which shows a restricted conformational movement is χ_1, which is localized around 180°. The ranges of these angles do not deviate from those allowed in the more extensive sampling in the 15 simulations where Asp195 was not restricted in its motion. The other torsional angles of TRH show similar distributions as in the other simulations.

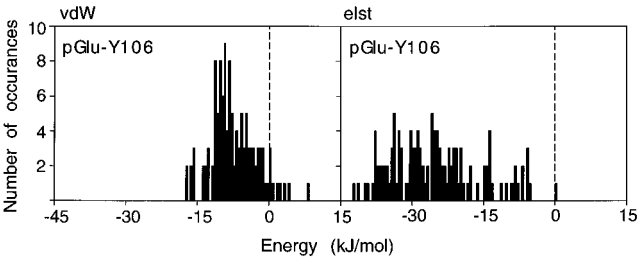

FIGURE 7: Distribution of pairwise nonbonded interaction energies divided into van der Waals (vdW) and electrostatic (elst) contributions from interaction of pGlu of the ligand with Tyr106 (Y106) in four simulations in which the side chain of Asp195 was interacting with Arg283.

This test implies that for Tyr106 to be able to form a H-bond to pyroGlu, Asp195 cannot be free and close to it; rather, a good interaction partner is required to prevent Asp195 from competing with pyroGlu for the interaction with Tyr106. The choice of Arg283 to anchor Asp195 away from Tyr106, while not based on experimental observations, provides a strong ionic interaction and is likely to keep Asp195 bound to it. An alternative suggestion is borne out from the minimized unoccupied receptor model (not shown) in which the hydroxyl of Tyr106 is H-bonded to the carboxylate of Asp195. Such an arrangement presents the possibility for maintaining the interaction between Asp195 and Tyr106 through a water molecule without competing for the H-bonding capability to pyroGlu. A water molecule could interact on the one hand with the carboxylate of Asp195 and on the other hand with the oxygen atom of the OH group of Tyr106. This maintains the interaction between Asp195 and Tyr106 but leaves the O−H group to form a H-bond to pyroGlu. At the present time there is no evidence to support these speculations, and further tests on the presence of interactions with Asp195 are in progress.

Other components of the interaction between pyroGlu and the receptor are a van der Waals attraction to Tyr106 and an electrostatic repulsion from Arg306. The interaction with Tyr106 has a mean value of -8.1 ± 3.0 kJ/mol and arises most often from interactions between the ring of Tyr106 and the apolar carbons of the pyroGlu ring. An interesting interaction between pyroGlu and Arg306 is the small but consistent electrostatic repulsion with a mean of 4.4 ± 2.6 kJ/mol. In our previous work, we have demonstrated that the O−H group of Tyr106 interacts with the C═O group of pyroGlu by replacing the pyroGlu with a Pro, which does not have the corresponding carbonyl. The observed reduction in affinity of the Pro^1 analog of TRH by nearly 100 000-fold, approximately 30 kJ/mol, suggests that such a change is larger than what can be accounted for by a loss of a hydrogen bond. The observed repulsion between pyroGlu and Arg306, although a secondary effect, could be a contributor to this large change because the positive charge on the nitrogen of the proline would increase the extent of the repulsive contribution to the change in affinity.

Histidine of TRH. In all simulations, the rings of Tyr282 and His were found to be in close proximity even though the relative positions of the two aromatic rings vary from parallel stacking to angled overlap. This correlates very well with the distribution of interaction energies between Tyr282 and His shown in Figure 6b. The van der Waals interaction energy is small but consistently negative, averaging at -9.6 ± 2.6 kJ/mol. In contrast, the electrostatic interaction energy is close to zero. Interestingly, there is a smaller but consistent van der Waals attractive interaction between His and Arg306 (-2.6 ± 1.9 kJ/mol), which originates from the aliphatic side chain of the Arg. In contrast, the distribution of electrostatic interactions between Arg306 and His (see Figure 6b) is repulsive, averaging around 12.0 ± 4.6 kJ/mol. The interaction originates from the repulsion between the guanidinium group of Arg306 and the imidazole ring of His. This is consistent with experimental results on the pH dependence of TRH binding to its receptor. We demonstrated in earlier studies (Perlman et al., 1992) that the binding at lower pH was diminished, and we were able to show that the pH dependence coincides with the pK_a of the imidazole ring. Thus, while there is no direct interaction between Arg306 and His, the electrostatic field of the positively charge guanidinium group plays an important potential role in affecting the binding of the protonated form of TRH at pH values below its pK_a. The experimental data on the interaction between histidine of TRH and Tyr282 (see preceding paper) are consistent with the observed stacking interactions.

Proline of TRH. The proline amide portion of TRH interacts only with Arg306 in HX 7. The major interaction is electrostatic in nature and represents the H-bond between the terminal C═O and the guanidinium of Arg306. The distribution of the pairwise interaction energies in individual structures at 310 K (see Figure 6c) shows that the contributions from van der Waals interactions are centered around -2.0 ± 2.3 kJ/mol, indicating the lack of importance of this interaction. The distribution of electrostatic interaction energies shows clearly two populations. The major one, constituting 80% of the structures in the simulations, is widely distributed and centered around -50 kJ/mol. These represent the H-bonded structures. The pattern of H-bonds varies because of the multiple possibilities of H-bonding to the guanidino group of Arg306. The wide distribution of the interaction energies reflects the different number of H-bonds formed between Arg306 and the $ProNH_2$. The other distribution is narrow and is centered around -5 kJ/mol, representing the 20% of the structures which do not have an H-bond between Arg306 and the $ProNH_2$. In some of the structures, Arg306 lies 6 Å above the ligand and does not form any contacts to TRH but interacts with Gln105 and Tyr192. In other structures, Arg306 is close to TRH and forms H-bonds to the backbone (see below), but the terminal carboxamide interacts with serines from helix 3 and helix 7. There are no current data to support these interactions. These results are consistent with the experiments in which the Arg306−$ProNH_2$ interaction has been identified as one of the specific receptor−ligand connections [see Perlman et al. (1996)].

Backbone of TRH. Most of the attention in structure−activity studies on TRH has concentrated on the side chains. In a small peptide as TRH, the backbone is expected to be mostly exposed and can be involved in interactions with the receptor. The distribution of pairwise interaction energies shown in Figure 6d indicates that van der Waals forces play no important role in the interaction between the backbone and the receptor. The electrostatic interaction energies suggest two recurring H-bonding partners for the backbone carbonyls: Tyr282 and Arg306. The distribution of the Tyr282 interaction energies with the backbone shows two populations. The broad distribution corresponds to the

hydroxyl group of Tyr282 binding to the C═O of pyroGlu in six of the simulations with an average strength of −30.2 ± 3.2 kJ/mol. The average electrostatic interaction energy in the rest of the runs is 0.4 ± 1.8 kJ/mol, indicating that in these simulations Tyr282 did not form a hydrogen bond with the backbone. The presence of the H-bond between Tyr282 and the backbone should be testable experimentally. Indeed, the effect of the Tyr282Phe mutation is an 8.3-fold reduction in affinity [see Perlman et al. (1996)]. The interaction could not be tested by eliminating the backbone C═O of the ligand, because such an analog was not available. An 8.3-fold reduction in affinity corresponds to loss of 5 kJ/mol in binding energy, which is much less than the 30 kJ/mol observed in the simulations. It should, however, be kept in mind that the pairwise interaction energies are not directly comparable with changes in affinities. The experimentally measured change in affinity includes possible loss of intrareceptor interactions in the unoccupied receptor resulting from the elimination of the OH group of Tyr282. In the unoccupied model of the receptor (not shown), Tyr282 is H-bonding to Tyr192. Thus, the energetic gain in forming the Tyr282−backbone H-bond is offset by breaking the hydrogen-bonding network of Tyr282 that existed in the receptor without the ligand. In the mutant receptor Tyr282Phe, no such H-bonds can exist, and the reduction in affinity due to loss of H-bonding to the ligand will be offset by the fact that no H-bonds need to be disrupted in the receptor.

Hydrogen bonds between the backbone carbonyls of TRH and Arg306 are the most frequently occurring interaction in the simulated structures. Only in one simulation is an H-bond between the two not present, resulting in a very small electrostatic interaction around −15 kJ/mol. On the other hand, most simulations show two H-bonds between the His peptidyl C═O and Arg306, and some show the guanidino group interacting with both backbone C═O groups of the ligand. The average strength of the interactions is −75.4 ± 19.6 kJ/mol. The multiple interactions between Arg306 and the backbone restrict the backbone mobility severely. They might be the most critical element in determining the conformation of the bound ligand. It should be possible to detect these interactions if analogs with a modified backbone were available. Recent design of a peptide mimetic of TRH based on a cyclohexane framework (Olson et al., 1995), which has no backbone carbonyls, may offer a possible test of the involvement of this part in ligand receptor interactions.

The backbone torsional angles in TRH that are free to rotate are ψ_1, ϕ_2, and ψ_2 (ψ_3 is considered to be part of the $ProNH_2$ group). As can be seen in Figure 5a the values of ψ_1 cover a wide range of angles with a broad maximum around 50° and two additional smaller populations around ±150°. This agrees with the proposed free rotation of this torsional angle based on NMR measurements (Feeney et al., 1974) but poses specific questions about the role of interactions between pyroGlu and Asn110. The population around 50° corresponds to structures that maintain an H-bond between the N−H of pyroGlu and the C═O group of the carboxamide of Asn110. In the other populations, the formation of this H-bond is more difficult, and when ψ_1 is in the range of −150°, the H-bond cannot form. Interestingly, in the simulations in which the side chain carboxylate of Asp195 was interacting with Arg283, the only observed population of ψ_1 was centered around 50°. This lends further support for the suggestion that Asp195 was acting as a competitive group for Tyr106, thus reducing the population of structures in which the interaction Tyr106−pyroGlu was maintained.

The backbone dihedral angles of His (ϕ_2 and ψ_2) populate only one conformation, as mentioned earlier and shown in Figure 5a. The distribution of ϕ_2 is wider than that of ψ_2, as shown by the mean and standard deviations of the distributions: $\phi_2 = -89.2° \pm 28.3°$ and $\psi_2 = -57.3° \pm 13.1°$. The backbone torsional angles of the receptor-bound TRH are thus close to an α-helical domain. This clearly differs from earlier experimental data (Donzel et al., 1974; Vicar et al., 1979), which led to the conclusion that the free TRH in solution is most likely in the extended conformation. These results raise the question whether the receptor recognizes TRH in its extended form and in the process of binding induces the conformational change or it recognizes and binds the folded form, which may be a minor population in solution. One way of addressing this question is by estimating the energy difference between the extended and the folded forms. In aqueous environment represented in MacroModel, the energy of the receptor-bound folded form is 52 kJ/mol higher than that of the extended form. Such an energetic difference would make the population of the folded form in aqueous solution too low to play an important role in being recognized by the receptor. We have to conclude that the receptor initially recognizes the extended form of TRH and subsequently induces the conformational change in the structure. Such a behavior would be consistent with the observation that the binding of TRH to its receptor exhibits a biphasic kinetics. As was demonstrated previously (Hinkle & Kinsella, 1982), the receptor-bound TRH can be characterized by a rapidly dissociating, low-affinity complex formed early in the binding process that changes into a slowly dissociating, high-affinity form. The rapidly dissociating form of the bound TRH would correspond to an early recognition low-affinity complex between the receptor and the extended form of TRH. The slowly dissociating form would correspond to the high-affinity complex formed between the receptor and the folded form of TRH. Since the interaction energy between Arg306 and the backbone of TRH is approximately −75 kJ/mol and Arg306 seems to be responsible for the restricted conformation of the backbone, this residue may induce the change in the conformation of TRH from an extended to the folded form found in the complex.

The energetic analysis allows us to generalize the discussion of the complex of TRH in its binding site from a residue−residue representation to the physical forces that govern these interactions. The residues of TRH and the experimentally identified key residues in the receptor that interact with each other show three different kinds of interaction, which can be characterized by their magnitude and directional requirements. The weakest and least directional interaction is the van der Waals attraction between His and Tyr282. The magnitude of the attraction is of the order of 10 kJ/mol, and it correlates with the shortest distance between the rings but is not dependent on the exact identity of the closest neighbors. In clear distinction, the polar H-bond between the tyrosines and the carbonyls (Tyr106−pyroGlu and Tyr282−backbone) is very restricted by distance and angle between the hydroxyl and the carbonyl groups.

Consequently, although the H-bond is rather strong (approximately 30 kJ/mol), it is relatively easily disrupted by structural changes in the ligand or in the binding pocket. The strongest interaction seen in the complex is the H-bond between the charged Arg306 and the carbonyl groups. These interactions, whether with the backbone carbonyls or with the $ProNH_2$ terminus, are nearly unbreakable and omnipresent with an average attraction of 50 kJ/mol. They function both in anchoring the ligand to the receptor and in inducing a particular backbone conformation to produce a folded form of the ligand, which is not available in solution but fits very well into the tight binding pocket in the receptor.

Structure(s) of the Ligand−Receptor Complex. The structures of the ligand−receptor complex produced in all the simulations cannot be pooled indiscriminantly to generate a representative consensus structure of the complex. The large conformational changes that are introduced by the Monte Carlo steps would prevent a simple averaging procedure. We had to establish criteria to select certain structures which would be representative and consistent with experimental observations. The experimental data regarding the involvement of Tyr106, Tyr282, and Arg306 in binding the ligand were used as the final criteria for choosing structures for a more detailed examination. Three simulations (3, 9, and 12 in Table 1) maintained the interactions of pyroGlu-Tyr106, His-Tyr282 and $ProNH_2$-Arg306 simultaneously. The final structures from these simulations were annealed from 310 to 10 K at a rate of 1 K/ps to eliminate large structural fluctuations. The three structures are referred to as **1**, **2**, and **3**, and they are shown in Figure 8.

The TRH in structure **1** in Figure 8A is anchored to the receptor through the interactions defined by the experimental studies. It has a strong H-bond between Tyr106 (in HX 3) and the ring C═O of pyroGlu. Asn110 (in HX 3) is positioned under the Tyr106−pyroGlu pair, and its side chain NH_2 makes an H-bond to the oxygen of Tyr106. The distance between the side chain C═O (Asn110) and the NH (pyroGlu) is 2.6 Å, and the angle N−H···O is 91.4°; both the distance and the angle are outside the range for an effective H-bond. However, the planes of the side chain amide of Asn110 and the ring imide of pyroGlu are nearly parallel, and their dipoles are almost perfectly aligned in an antiparallel direction with an angle between the dipoles of 170°. Asp195 in HX 5 interacts with the ring N−H of Trp150 and the OH group of Thr153 both from HX 4 and does not interfere with the Tyr106−pyroGlu interaction. The histidine of TRH lies under Tyr282 (in HX 6), forming an effective stacking interaction. The OH of Tyr282 makes an H-bond with the backbone C═O of pyroGlu, and the OH of Tyr192 (in HX 5) makes an H-bond to the oxygen of Tyr282. The His side chain of TRH is surrounded by Leu274, Trp279 (both in HX 6), Asn312, and Ser313 (both in HX 7). The carboxamide terminus of proline is H-bonded to Arg306 (in HX 7), which in turn interacts with Tyr192. The terminal NH_2 group of the proline is positioned between three polar groups that can act as H-bond acceptors. Asp71 from HX 2 and Ser112 from HX 3 make good H-bonding interactions with this group. From HX 7, the OH of Tyr310 is positioned close to the NH_2 group at a distance of 2.95 Å. The OH of Tyr310 acts as a H-bond donor in its interaction with Asp71. The hydrophobic part of the side chain of proline, $C_\beta C\gamma C_\delta$, sits packed between the side chains of Ile109, Ser113, and Ile116 from HX 3 and Ser313 and Asn316 from HX 7.

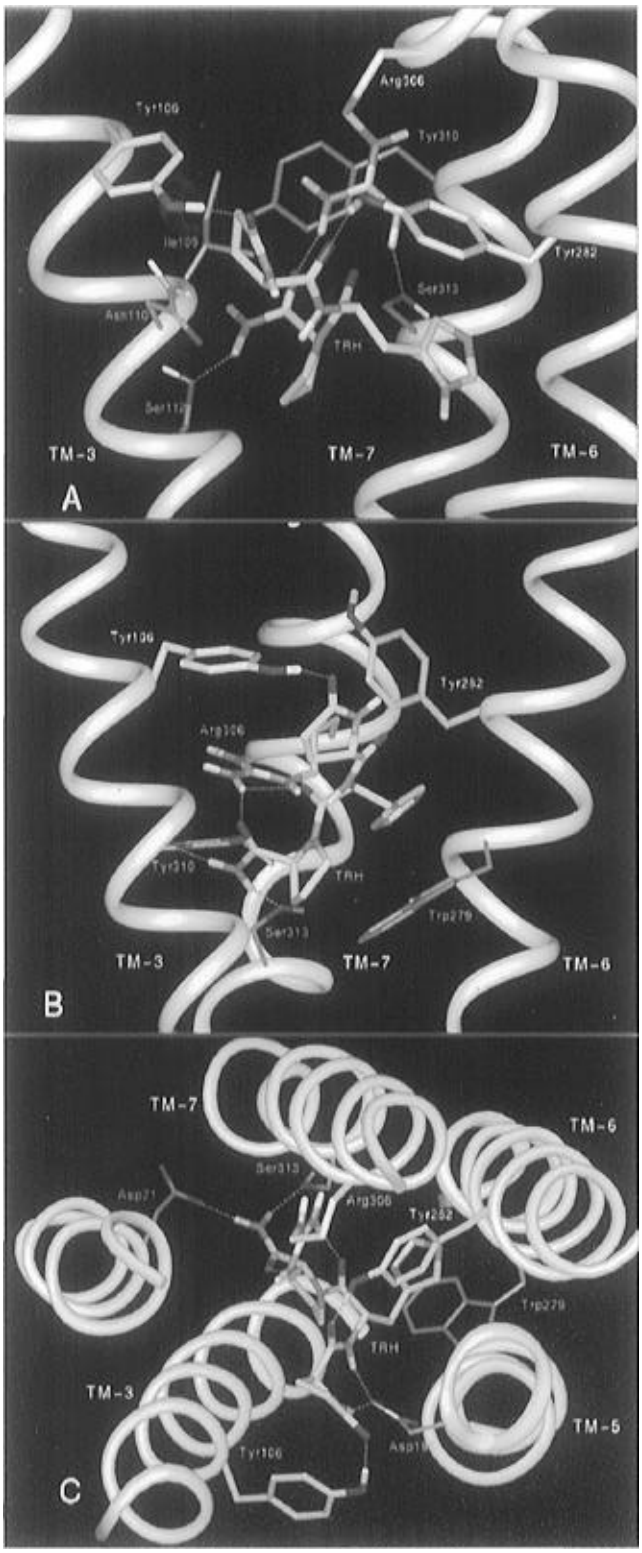

FIGURE 8: Close-up views of the three structures selected from the simulation that maintain simulataneous interaction with Tyr106, Tyr282, and Arg306 (colored in white). Additional residues observed in the vicinity of the ligand are colored orange. The TRH is in yellow. For clarity not all the helices are shown. Panels: (A) structure **1**; (B) structure **2**; (C) structure **3** (top view).

Mutations of these residues to alanines should help binding of crowded analogs.

The ring C═O of pyroGlu in structure **2** in Figure 8B is 1.64 Å away from the OH of Tyr106 forming a strong H-bond. This structure differs from structure **1** primarily in the torsional angle ψ_1, which is −155° rather than 137° as

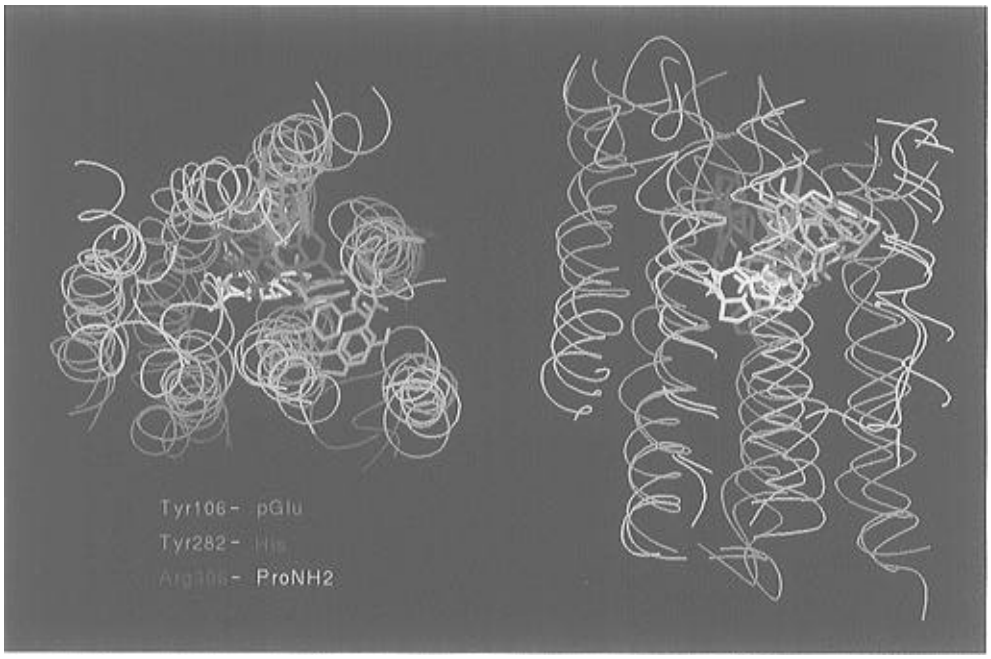

FIGURE 9: Superposition of the three structures showing a top view (left) and a side view (right). The structures were superimposed On the basis of the TM helices.

in structure **1**. Consequently, the ring N−H turns in the opposite direction, moving away from Asn110 to a distance of 11.5 Å. The ring N−H is now positioned in the vicinity of the backbone carbonyls of Ile191 and Tyr192. However, we do not attribute any significance to these interactions because of the partial unwinding of the top of HX 5, which exposed these groups for interaction with the ring N−H. The ring of Tyr106 is proximal to the aliphatic carbons of pyroGlu contributing to a van der Waals interaction. The imidazole ring of His is close to one edge of Tyr282, forming a nearly perpendicular interaction rather than a stacked one. Several hydrophobic residues from HX 5 (Phe 196) and HX 6 (Leu274 and Leu278) are within van der Waals distance to the imidazole ring. The terminal C═O of the $ProNH_2$ forms an H-bond with Arg306, and the NH_2 group interacts with the OH groups of Tyr310 and Ser313 in HX 7. The $C_\beta C_\gamma$ bridge of $ProNH_2$ makes van der Waals interactions with the side chains of Ser112 and Ile116. The backbone carbonyl of pyroGlu forms an H-bond with the backbone HN of Tyr192 (however, see above), and the backbone carbonyl of His attracts the OH of Tyr192 to a distance of 1.68 Å and the guanidino group of Arg306 to a distance of 1.72 Å.

In structure **3** shown in Figure 8C, similarly to the other structures, the C═O of pyroGlu is H-bonded to the OH group of Tyr106 at a distance of 1.73 Å. Also, as in structure **2**, the H-bond to Asn110 is disrupted, placing it about 10 Å away from pyroGlu. However, in structure **3** the reason for this is different than in structure **2**. In this structure ψ_1 is 59°; thus the orientation of the pyroGlu ring is not entirely rotated with respect to Asn110. Instead, the carboxylate of Asp195 forms a H-bond with the ring N−H of pyroGlu at a distance of 1.75 Å. It also interacts with the backbone N−H group of the His. This is another instance of the competing effect of Asp195 on the position of the ring of pyroGlu. Similarly to previous structures the ring of Tyr106 forms van der Waals interactions with the C_β−C_γ edge of pyroGlu. His of the ligand in this structure also forms an edge interaction with Tyr282. Additional residues that are in close proximity to His are Phe196, Leu274, and Ile309. The C═O of $ProNH_2$ forms a strong H-bond with Arg306 at a distance of 1.72 Å. The NH_2 group of the terminal carboxamide is anchored between the O_δ of Asp71 in HX 2 and the OH group of Ser313 in HX 7 and is 3.3 Å from the OH group of Tyr310. The C_γ of Ile109 in HX 3 is within 3.3 Å to the aliphatic carbons of the proline ring. The backbone C═O of pyroGlu is H-bonded to the OH of Tyr282 at a distance of 1.7 Å, and that of His is H-bonded to the guanidino group of Arg306 at a distance of 1.75 Å.

In addition to the similar interactions with the three residues which were identified in experiments and used to select the three structures, the TRH interacts with a few additional common residues. Two Ile residues in HX 3 (109 and 116) are consistently found to interact with the aliphatic carbons of the proline ring. It would be of interest to mutate these residues to alanines and test the effect of mutation by a complementary change in the proline ring. Two residues in HX 7, Tyr310 and Ser313, are also consistently found to interact with the NH_2 group of the $ProNH_2$. Recent preliminary results of mutating Tyr310 show that this residue affects the binding of TRH to its receptor.

The variability in the selected structures illustrates the importance of the transition from the structural model derived by a minimization procedure (see previous paper) to that presented here. To demonstrate the extent of the flexibility of the ligand and the receptors, the three structures were superimposed according to the C_α trace of the helices. The superposition, shown in Figure 9, demonstrates the extent of structural flexibility in the ligand and in the receptor that can satisfy the required connections in the complex. It emphasizes the dynamic nature of the interaction between the ligand and the receptor. In other words, the three structures illustrate not only the outcome of three simulations but also the accessible structures of the complex due to the flexibility of the ligand and the receptor. Even though the process of ligand dissociation from the receptor cannot be modeled because of the partial description of the receptor and the absence of an environment into which the ligand

could transfer, the observed flexibility is one of the necessary conditions for the dissociation of the ligand−receptor complex.

CONCLUSION

Structural hypotheses about receptor recognition and activation require a molecular model of the ligand−receptor complex. Only with a structure at an atomic resolution can one test the feasibility of hypothesized interactions, both by rationalizing experimental results and by predicting new possible interactions for future testing and refinement. At the present time, no experimental structures of the G-protein-coupled receptors are available. Thus, the only way to gain structural insights of GPCR structure and function is to use molecular models. The present work demonstrates that a careful construction of models, based on experimental data, can provide a powerful tool in formulating the molecular basis for receptor selectivity.

The model constructed in this work proved to be sufficiently stable to be used in high-temperature mixed mode Monte Carlo/stochastic dynamics simulations. The choice of including a large set of torsional angles in the Monte Carlo-active zone allowed for a very good sampling of the conformational space of the ligand and the binding pocket in the receptor. The interactions between Arg306 and $ProNH_2$ and between Tyr282 and His were present in most of the simulations. The stability of the Arg306−$ProNH_2$ interaction is probably caused by both the strength of the ionic H-bond and the flexibility of Arg side chain. Although the Tyr282−His interaction is weak, the lack of strong directional forces of van der Waals attractions makes it an important contribution to affinity. The strong but directionally restricted H-bond between pyroGlu and Tyr106 may be affected by the residues around Tyr106.

The model, however, should not be considered as a final product but rather a reflection of the present stage of knowledge. As such, it identified new residues in the vicinity of the binding pocket that may be very important for receptor function. We have shown that Asp195 can compete with pyroGlu for the H-bond to Tyr106. The suggestion that Asp195 is anchored to another part of the receptor is an interesting hypothesis that will be tested experimentally. Interactions between the aliphatic carbons in the rings of pyroGlu and Pro and hydrophobic residues in the receptor are new contacts that are proposed for testing. Preliminary results from mutations of Tyr310 in helix 7 support the observed interaction with the C-terminal NH_2 group. Among the most important conclusions from this study is that the simulations give an estimate of the mobility of the ligand and the binding site, and they describe the known interactions in molecular biophysical terms.

REFERENCES

Chalmers, D. K., & Marshall, G. R. (1995) *J. Am. Chem. Soc. 117*, 5927−5937.

Donzel, B., Rivier, J., & Goodman, M. (1974) *Biopolymers 13*, 2631−2647.

Feeney, J., Bedford, G. R., & Wessels, P. L. (1974) *FEBS Lett. 42*, 347−351.

Guarnieri, F. (1995) *J. Math. Chem. 18*, 25−35.

Guarnieri, F., & Still, W. C. (1994) *J. Comput. Chem. 15*, 1302−1310.

Hinkle, P. M., & Kinsella, P. A. (1982) *J. Biol. Chem. 257*, 5462−5470.

Kirkpatrick, S., Gelatt, C. D. J., & Vecchi, M. P. (1983) *Science 220*, 671−680.

Laakkonen, L., Li, W., Perlman, J. H., Guarnieri, F., Osman, R., Moeller, K. D., & Gershengorn, M. C. (1996) *Mol. Pharmacol. 49*, 1092−1096.

Leach, A. R. (1994) *J. Mol. Biol. 235*, 345−356.

Lybrand, T. P. (1995) *Cur. Opin. Struct. Biol. 5*, 224−228.

McCammon, J. A., & Harvey, S. C. (1987) *Dynamics of Proteins and Nucleic Acids*, Cambridge University Press, New York.

Metropolis, N., Rosenbluth, A. W., Rosenbluth, M. N., Teller, A. H., & Teller, E. (1953) *J. Chem. Phys. 21*, 1087−1092.

Mohamadi, F., Richards, N. G. J., Guida, W. C., Liskamp, R., Lipton, M., Caufield, C., Chang, G., Hendrickson, T., & Still, W. C. (1990) *J. Comput. Chem. 11*, 440.

Olson, G. L., Cheung, H.-C., Chiang, E., Madison, V. S., Sepinwall, J., Vincent, G. P., Winokur, A., & Gary, K. A. (1995) *J. Med. Chem. 38*, 2866−2879.

Perlman, J. H., Nussenzveig, D. R., Osman, R., & Gershengorn, M. C. (1992) *J. Biol. Chem. 267*, 24413−24417.

Perlman, J. H., Laakkonen, L., Osman, R., & Gershengorn, M. C. (1994a) *J. Biol. Chem. 267*, 23383−23386.

Perlman, J. H., Thaw, C. N., Laakkonen, L., Bowers, C. Y., Osman, R., & Gershengorn, M. C. (1994b) *J. Biol. Chem. 269*, 1610−1613.

Perlman, J. H., Laakkonen, L., Osman, R., & Gershengorn, M. C. (1995) *Mol. Pharmacol. 47*, 480−484.

Perlman, J. H., Laakkonen, L. J., Guarnieri, F., Osman, R., & Gershengorn, M. C. (1996) *Biochemistry 35*, 7643−7650.

Rosenfeld, R., Zheng, Q., Vajda, S., & C., D. (1993) *J. Mol. Biol. 234*, 515−521.

Swope, W. C., Andersen, H. C., Berens, P. H., & Wilson, K. R. (1982) *J. Chem. Phys. 76*, 637−649.

Vicar, J., Abillon, E., Toma, F., Pirou, F., Litner, K., Bláha, K., Fromageot, P., & Fermandjian, S. (1979) *FEBS Lett. 97*, 275−278.

Weiner, P. K., & Kollman, P. A. (1981) *J. Comput. Chem. 2*, 287−303.

Weiner, S. J., Kollman, P. A., Case, D. A., Singh, U. C., Ghio, C., Alagona, G. A., Profeta, S. J., & Weiner, P. (1984) *J. Am. Chem. Soc. 106*, 765−784.

Yamada, N., & Itai, A. (1993a) *Chem. Pharm. Bull. (Tokyo) 41*, 1203−1206.

Yamada, N., & Itai, A. (1993b) *Chem. Pharm. Bull. (Tokyo) 41*, 1197−1202.

Zacharias, M., Luty, B. A., Davis, M. E., & McCammon, J. A. (1994) *J. Mol. Biol. 238*, 455−465.

BI952203J